Hindawi Publishing Corporation
Advances in Power Electronics
Volume 2015, Article ID 587197, 9 pages
http://dx.doi.org/10.1155/2015/587197

Research Article

Design and Implementation of Three-Level DC-DC Converter with Golden Section Search Based MPPT for the Photovoltaic Applications

Chouki Balakishan, N. Sandeep, and M. V. Aware

Visvesvaraya National Institute of Technology, Nagpur 440010, India

Correspondence should be addressed to N. Sandeep; sandeep.1991.in@ieee.org

Received 11 August 2014; Revised 12 December 2014; Accepted 30 December 2014

Academic Editor: Pavol Bauer

In many photovoltaic (PV) energy conversion systems, nonisolated DC-DC converters with high voltage gain are desired. The PV exhibits a nonlinear power characteristic which greatly depends on the environmental conditions. Hence in order to draw maximum available power various algorithms are used with PV voltage/current or both as an input for the maximum power point tracking (MPPT) controller. In this paper, golden section search (GSS) based MPPT control and its application with three-level DC-DC boost converter for MPPT are demonstrated. The three-level boost converter provides the high voltage transfer which enables the high power PV system to work with low size inductors with high efficiency. The balancing of the voltage across the two capacitors of the converter and MPPT is achieved using a simple duty cycle based voltage controller. Detailed simulation of three-level DC-DC converter topology with GSS algorithm is carried out in MATLAB/SIMULINK platform. The validation of the proposed system is done by the experiments carried out on hardware prototype of 100 W converter with low cost AT'mega328 controller as a core controller. From the results, the proposed system suits as one of the solutions for PV based generation system and the experimental results show high performance, such as a conversion efficiency of 94%.

1. Introduction

The photovoltaic systems are major contributors in the electrical power. These are utilized effectively with interface to the existing systems through DC-DC converters. The major challenge is to extract the power under varying operating conditions which influence the output voltage [1, 2].

Isolated converter structures with cascaded configuration enables to achieve high voltage gain [3]. However, these are used up to several kW applications [4, 5]. The multilevel buck converters proposed are widely used in high frequency DC/DC power conversion [6, 7]. In the conventional boost converters, high voltage ratio is feasible without multistage cascading [8]. The voltage ratios in these are limited by the parasitic elements and switching control used [9, 10]. Three-level boost converters have significant advantage as compared to conventional boost converter. The size of the inductor is reduced and switch voltage rating is half of the output voltage. This reduces the overall size and improves the efficiency in three-level DC-DC converters. However, the voltage balancing across the DC bus capacitors is required due to nonidealities in the components. This is feasible by sensing the voltages across them with corrective feedback through controllers [11, 12]. The current sensing of inductor by dispensing the voltage measurements is feasible to balance the voltages across the DC bus capacitors [13].

PV array in solar power conversion system operates at a point having maximum power transfer. It is necessary to track this operating point by using the MPPT control algorithms to maximize the utilization efficiency. Various algorithms for MPPT are reported in the literature and used for the efficient energy conversion process [14]. These methods are derivative based and noise sensitive. A computational ease with inherent robust MPPT using golden section search (GSS) based algorithm is proposed in this paper. This is having noise and signal fluctuation immunity with fast convergence as compared to many reported MPPT methods [15, 16]. This GSS based MPPT method is easy to implement on the low cost hardware

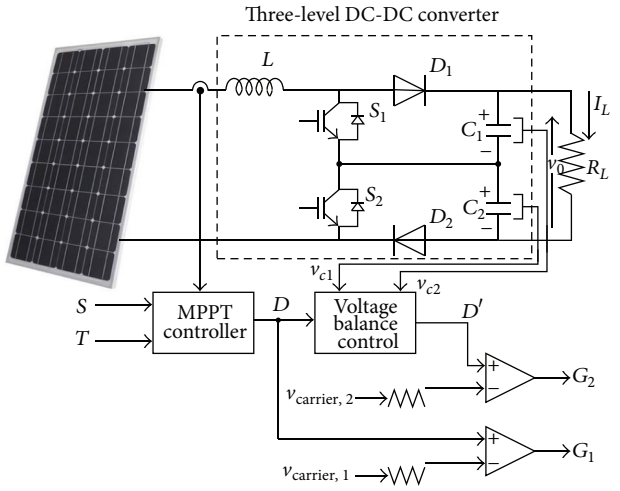

Figure 1: Proposed scheme with PV-fed three-level boost converter.

with single current sensor. The PV connected system with three-level converter using GSS based MPPT is presented in Figure 1.

In this paper, GSS MPPT based three-level DC-DC boost converter for PV energy conversion system is presented. A simple duty cycle based pulse width modulation (PWM) and capacitor voltage controller are suggested. The switching and reverse recovery losses are less in the three-level boost converter. A hardware prototype of 100 W converter is built and the control is made cost effective using AT'mega based low cost controller. The steady state and dynamic behavior of the system are presented. Both the simulation and hardware results are seen to have clear agreement with inherent robustness built using new MPPT algorithm.

2. Three-Level Nonisolated DC-DC Converter

In high power rating PV systems with high voltage gain requires boost converter with controller to maintain the DC bus voltage constant. The interfacing PV with wide range of voltages with boost converter having three-level is advantageous due to reduce input filter size and current ripple cancellation. In three-level boost converter, switching devices voltage rating is half of the output voltage; this leads to increase the power density, efficiency, and reduction in cost. The three-level boost converter is shown in Figure 2. The voltage of the center point is $V_o/2$ as capacitors C_1 and C_2 are equal, which in turn reflects the voltage stress reduction across the switching devices in these converters.

2.1. Operating Principle. Symmetrical operation of three-level boost converter is explained with its operating modes. In this converter v_{c1}, v_{c2} are the voltage across the capacitors C_1, C_2, respectively. The switch S_1 is upper switch and S_2 is lower switch and switching frequency is f_s. In this converter, carrier signals $v_{\text{carrier},1}$ and $v_{\text{carrier},2}$ for PWM generation are triangular for both switches but those are in 180° phase shift to each other. With these carrier signals both switches can be turning ON and OFF at the same time. Therefore, the converter operates in four distinct modes as shown in Figure 3.

(1) Mode 1: both switches are turn ON as shown in Figure 2(a) and the voltage across inductor is (v_L) = input voltage ($v_{\text{in}} > 0$). In this mode the inductor is always in charging mode and charged capacitors supply the current to the load.

(2) Mode 2: in this mode S_1 is ON and S_2 is OFF as shown in Figure 2(b) and voltage across the inductor is $v_L = v_{\text{in}} - v_{c2}$. In this mode inductor may be in charging mode or discharging mode and charged capacitor C_1 supplies the current to the load while C_2 is in charging mode.

(3) Mode 3: in this mode, S_1 is OFF and switch S_2 is ON as shown in Figure 2(c) and voltage across the inductor is $v_L = v_{\text{in}} - v_{c1}$. In this mode inductor may be in charging mode or discharging mode and charged capacitor C_2 supplies the current to the load while C_1 is in charging mode.

(4) Mode 4: both switches are turned OFF as shown in Figure 2(d) and inductor voltage is $v_L = v_{\text{in}} - v_{c2} < 0$. Due to boosting operation $v_{c1} + v_{c2} > v_{\text{in}}$, so in this mode inductor always is in discharging mode and both capacitors are in charging mode and input supplies the current to the load.

In modes 1 and 4 inductor is in charging mode and discharging mode, respectively, but in modes 2 and 3 inductor currents raising polarity depend on the voltages v_{c1} and v_{c2}, depending upon the relation between v_{in} and half of the output voltage ($v_0/2$); there exist two operating regions.

(1) Region 1: $v_{\text{in}} > v_0/2$.

(2) Region 2: $v_{\text{in}} < v_0/2$.

In region 1, $v_{\text{in}} > v_0/2$; hence $v_L = v_{\text{in}} - v_0/2 > 0$ so inductor current raising polarity is positive in modes 3 and 2 as shown in Figure 3(a). This will occur only when duty ratios of upper switch (D_1) and of lower switch (D_2) are less than 0.5; in this region both switches must not be ON at the same time. In region 2, $D_1 = D_2 > 0.5$; input voltage is $v_{\text{in}} < v_0/2$; then, inductor current raising polarity is negative $v_L = v_{\text{in}} - v_0/2 < 0$ in modes 2 and 3 as shown in Figure 3(b). In this region both switches must not be OFF at the same time.

3. Current Ripple and Efficiency

In boost converter, maximum inductor current ripple ($\Delta i_{\max}$) occurs when duty ratio (D) is 0.5; at this duty ratio $v_{\text{in}} = 0.5v_o$. The inductor current ripple is given by

$$\Delta i_{\max} = \frac{v_{\text{in}}}{L} D T_s = \frac{V_0 T_s}{L}. \quad (1)$$

In three-level boost converter, equivalent switching frequency is twice the switching frequency of conventional boost converter. In region 1 maximum ripple occurs at $v_{\text{in}} = 0.25v_o$ and is given by

$$\Delta i_{\max} = \frac{v_{\text{in}}}{L} D T_s \frac{1}{2} = \frac{V_0 T_s}{16L}. \quad (2)$$

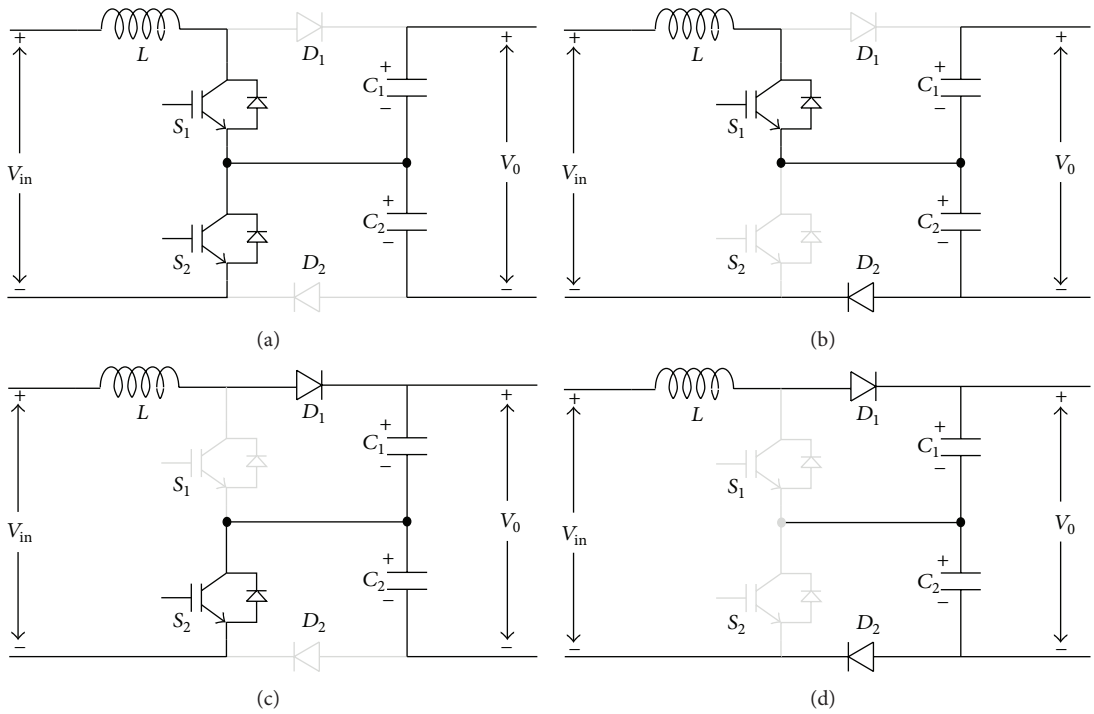

FIGURE 2: Operating modes of three-level DC-DC converter.

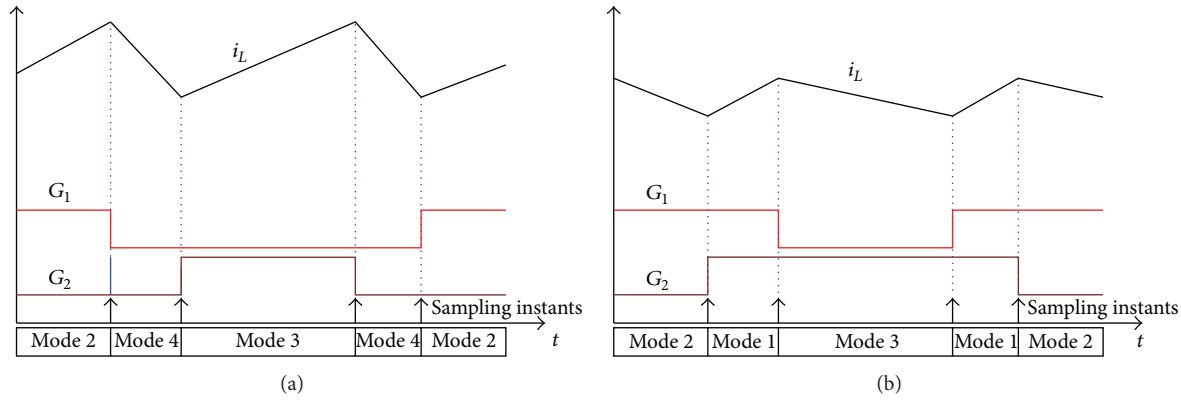

FIGURE 3: Operation waveforms. (a) Region 1. (b) Region 2.

From (1) and (2), it is observed that the inductor current ripple is less for three-level boost converter for the same inductor value and inductor value is four times less than conventional boost converter. The inductor loss due to the resistance is a major design parameter. The selection of the L/R ratio and switching devices losses are the major contributors in the efficient operation of the converter.

4. Proposed MPPT Scheme

In this MPPT technique, maximum power is tracked by controlling PV current to maximum power point current, which is computed by golden section search (GSS) algorithm. This GSS based MPPT needs to sense the irradiance, temperature, and PV current to maximize the power output from PV systems.

4.1. Golden Section Search Principle. The golden section search is a technique for finding extremum (minimum or maximum) by sequentially narrowing the range of values inside which extremum exists. The main aim is to find maximum functional value of $f(x)$ within the input interval $[a \;\; b]$. Two points x_1 and x_2 are selected in the interval $[a \;\; b]$ and function $f(x)$ is evaluated at these points. Points x_1 and x_2 are selected such that each point subdivides interval into two parts and length of whole line/length of larger fraction = length of larger fraction/length of smaller fraction. Assume a line segment [0, 1] as shown in Figure 4(b). Then $1/r = r/1-r$; that is, $r2 + r - 1 = 0$; hence $r = 0.618$.

Consider $x_1 = b-r(b-a)$; that is, x_1 is 0.618 of interval away from b.

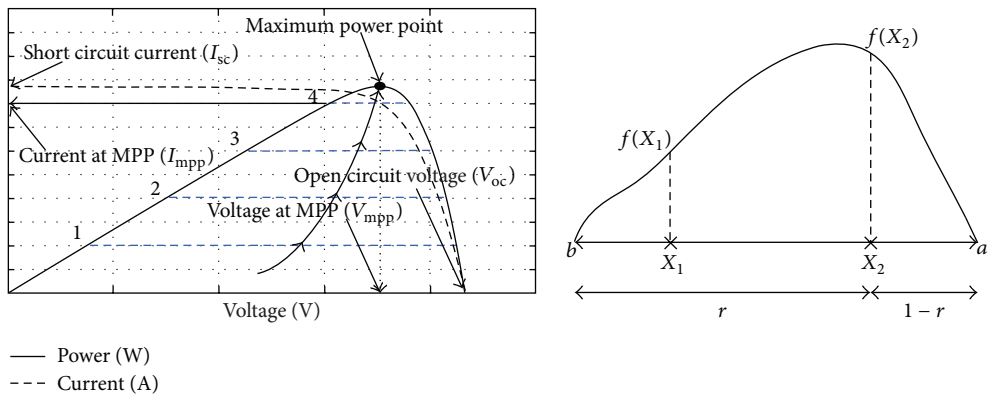

Figure 4: (a) MPPT tracking with GSS algorithm. (b) Division of interval on the characteristics.

Consider $x_2 = a+r(b-a)$; that is, x_2 is 0.618 of interval away from a.

For a GSS based MPPT for photovoltaic system, the P-V characteristics are the operating characteristics wherein $f(x)$ corresponds to power, whose maximum value has to be tracked. The range of operation is from zero to open circuit voltage (V_{oc}); that is, $a = 0$ and $b = V_{oc}$ as shown in Figure 4(b). The way of tracking maximum point is shown in Figure 4(a). The voltage corresponding to the maximum power is obtained and mapped into the V-I characteristics to obtain the current reference.

4.2. Golden Section Search Algorithm Based MPPT. MPPT is used to track the maximum power under different atmospheric conditions; this method is robust and also has a fast response as compared to the conventional MPPT algorithms. This algorithm has guaranteed convergence under continuous variable irradiance and temperatures. This GSS based MPPT has two parts; one is PV emulator which plots the PV characteristics for given irradiance and temperature by using mathematical model equations of PV cell; this requires solar PV parameters, irradiance, and temperature. The algorithm for generating the PV characteristics is presented in Figure 5(a).

The description of the parameters in the flow chart is as follows:

I_{sc}: short circuit current,

R_s: series resistance,

N_s: the number of cells of the array connected in series,

K_i: temperature coefficient of current,

a: ideality factor of diode,

q: carrier charge,

S_n: nominal irradiance,

T_n: nominal temperature,

E_g: band energy,

S: irradiance,

T: temperature,

I_0: photovoltaic saturation current.

The second part of the algorithm is to find the PV current at maximum power point (MPP) is shown in Figure 5(b).

The inductor current feedback is used to generate the error by comparing it with the reference current I_{MPP} generated by the GSS algorithm and it is processed through proportional (P) controller. This P controller changes the duty ratio (D) according to error and governs the PV to track the maximum power point on its characteristics. Figure 6 shows the block diagram of GSS MPPT based reference generator.

4.3. Voltage Balancing Control. Capacitors C_1 and C_2 are alternatively charged to their voltages v_{c1} and v_{c2}. Even though both capacitor values are equal, there is a voltage unbalance between output capacitors due to mismatch of two real capacitors and equivalent series resistance. The voltage balancing controller is required to maintain the equal voltages across these capacitors through duty cycle control and is implemented as shown in Figure 7. G_1 and G_2 are the gate pulses for switches S_1 and S_2, respectively. In the three-level boost operation of the DC-DC converters with duty ration relates the fact that the input and output voltage are given as

$$\frac{V_0}{V_{in}} = \frac{1}{1 - 0.5d_1 - 0.5d_2}. \tag{3}$$

If $d_1 = d_2 = D$, then

$$\frac{V_0}{V_{in}} = \frac{1}{1 - D}, \tag{4}$$

where the input DC voltage V_{in} is PV input voltage and varies with respect to varying environmental conditions. The duty ratio of the boost switch S_1 is determined by the MPPT control (D) and duty ratio of the boost switch S_2 is determined by the additional controller. The PI generates

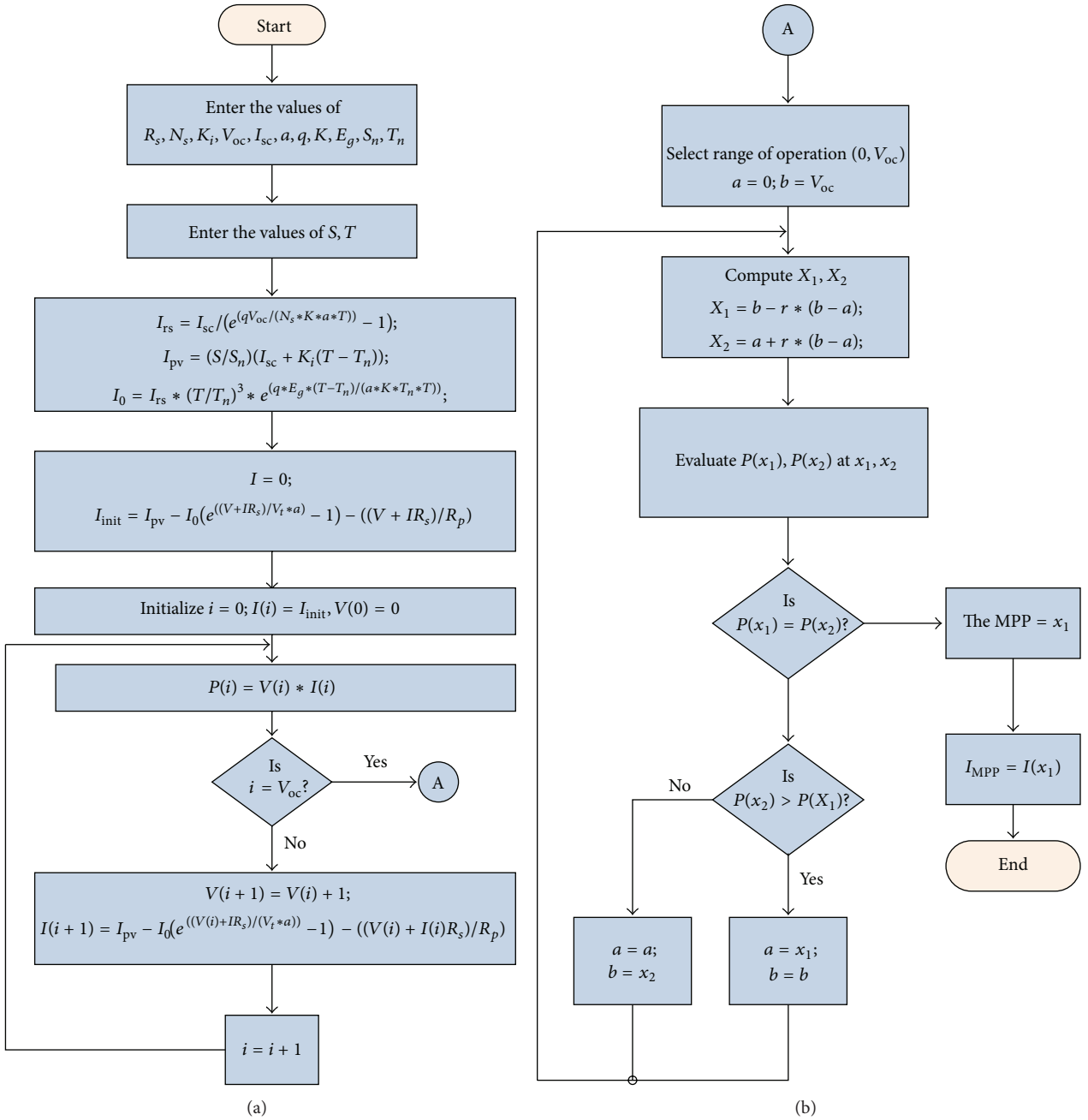

Figure 5: GSS MPPT flowchart: (a) PV emulator and (b) GSS method.

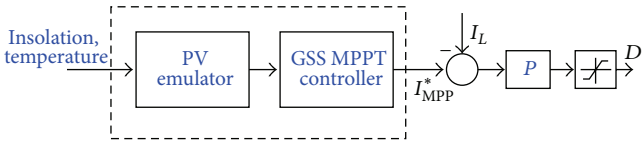

Figure 6: GSS MPPT control technique.

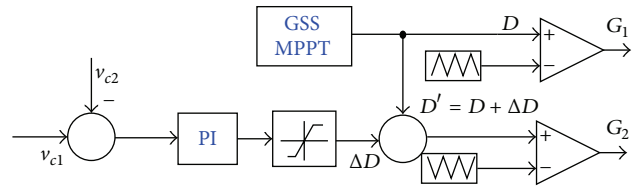

Figure 7: Block diagram of MPPT with voltage balance control.

the duty (D) from the voltage error obtained from $(v_{c1} - v_{c2})$. Consider

$$\Delta D = K_p + \frac{K_i}{s}\left(v_{c1} - v_{c2}\right), \tag{5}$$

where $K_p + K_i/s$ is the transfer function of the PI controller. The duty cycle $D' = D + \Delta D$ controls switch S_2 of the converter to balance the voltage across the capacitors.

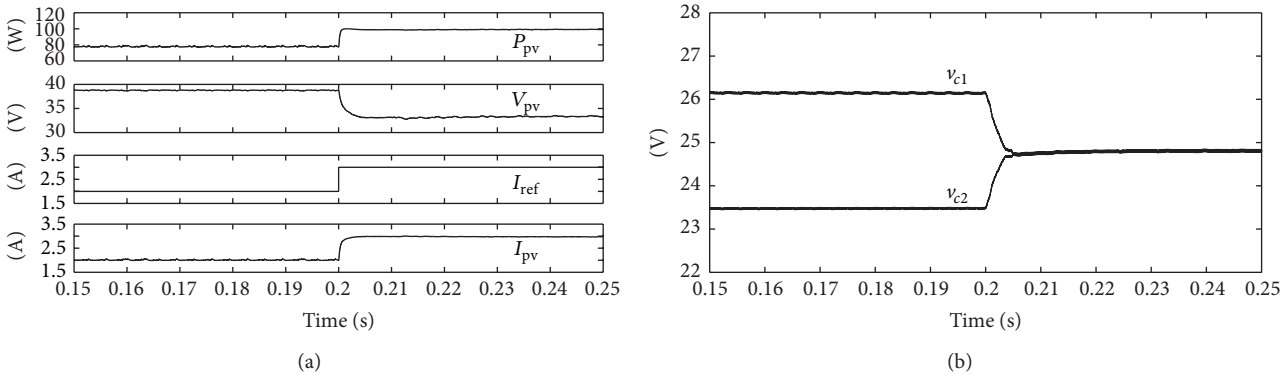

Figure 8: (a) Maximum power tracking at $S = 1000\ \text{W/m}^2$ and $T = 298$ K. (b) Voltage balancing under steady state.

Table 1: Specifications of the solar panel.

Maximum power (P_{mpp})	100 W
Voltage at maximum power point (V_{mpp})	34 V
Current at maximum power point (I_{mpp})	2.94 A
Short circuit current (I_{sc})	3.17 A
Open circuit voltage (V_{oc})	42 V

Table 2: Specifications of the hardware prototype.

Parameter	Value/part number
Inductor (L)	1.4 mH, 0.8 Ω
Capacitor (C_1 and C_2)	1000 μF
Switching frequency (f_{SW})	30 kHz
Power MOSFETs	IRFP250 (200 V, 30 A)
Hyperfast power diodes	1200 V, 8 A

5. Simulation Results

In this section, the converter operation with the MPPT control and voltage balancing is presented through simulation. The PV panel parameters are given in Table 1. The boost converter is operated with MOSFET switches and the details of the component specification are given in Table 2. The steady state and dynamic operation are presented for the various operating conditions.

5.1. Steady State Operation. The simulated results under steady state are shown in Figure 8. The PV panel is operating at a temperature 298 K with irradiation level of $1000\ \text{W/m}^2$. The converter operation with MPPT control and capacitor voltage balance activation at 0.2 s is presented in Figure 8(a). Initially reference value is set to 2 A (without MPPT); after that it is changed according to GSS MPPT. Then power drawn from the PV is increased to 100 W by controlling the PV cell current to the reference value generated by GSS MPPT algorithm. The DC bus capacitor voltage balance control is also presented with forced unbalance created by choosing the different values of C_1 and C_2 ($C_1 = 1000\ \mu$F and $C_2 = 900\ \mu$F). The voltages across these capacitors are maintained at the same value after the balancing; the voltage converges to a 23.5 V within the 0.02 s, while converter is operating in a maximum power tracking mode shown in Figure 8(b). This indicates the operation of the designed controller is effectively maintaining the power near to 100 W at the 50 V output through the duty ratio control at 30 kHz switching frequency.

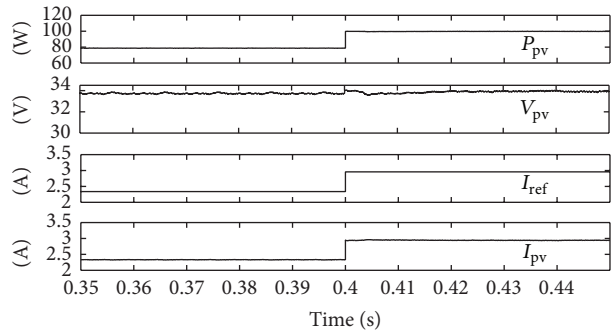

Figure 9: Maximum power tracking under step change in irradiance.

5.2. Dynamic Operation of the Converter. The MPPT algorithm with converter under varying irradiation levels and various loading condition is tested. The MPPT with a change in the irradiation level from $800\ \text{W/m}^2$ to $1000\ \text{W/m}^2$ is presented in Figure 9.

The voltage variation across the capacitors due to sudden loading on the converter (around 20% variation) is presented in Figure 10. It is observed that the voltage is controlled after the load variation and maintained to 23.5 V across each of the capacitors.

5.3. Performance Comparison with Other MPPT with Partial Shading. The proposed MPPT method is compared with Perturb and Observe and Incremental Conductance based MPPT techniques. The performance is evaluated under the partial shading. The partial shading *P-V* characteristics are used to test the performance with local and global peak as given in Figure 11.

The reference voltage (V_{ref}) generated by these methods are given in Figure 12 with the number of iterations required

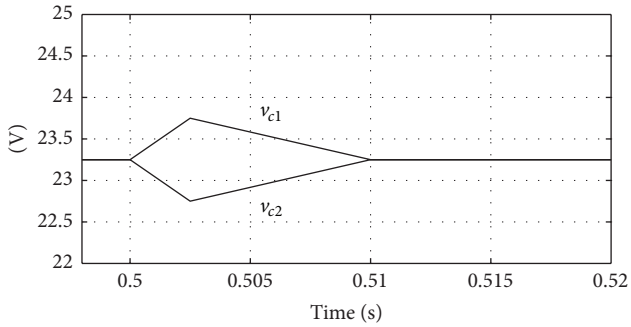

FIGURE 10: Voltage balancing under load change.

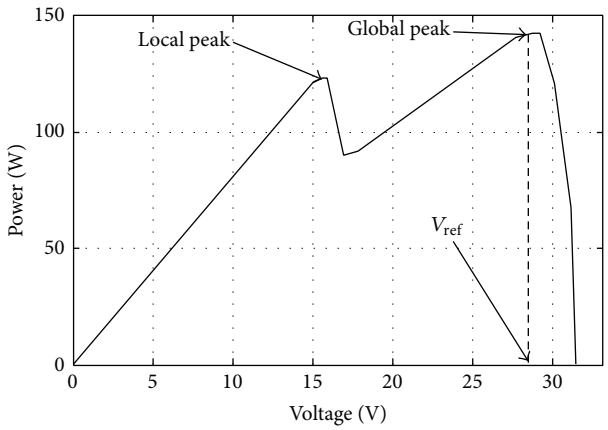

FIGURE 11: *P-V* characteristics under partial shading.

by these methods. It is observed that the iterations required for the GSS are 4-5 nos. as other methods take 7-8 nos. The variation in the generated reference is stable in GSS as it is tracking the local and global peak.

6. Experimental Results

The proposed scheme is implemented in AT'mega328 controller with GSS based MPPT and duty ratio control. The parameters of the hardware are built with the same parameters as given in Table 2.

6.1. Hardware Circuit Description. The block diagram of hardware prototype built is shown in Figure 13. The DC/DC converter is built with the MOSFET IRFP250. The interfacing drivers with isolation circuit using TLP350 are built. The capacitor voltage is sensed using voltage sensor LV-25P and inductor current by current sensor (WCS 2705). The controller AT'mega328 with built-in ADC is used to execute the MPPT algorithm and also the PI controller. The I/O pins are interfaced with the driving circuit to activate the switching devices. The photograph of the hardware prototype built is shown in Figure 14.

Figure 15 shows the measured power generated by PV and current and voltage across it. The PV current is controlled to maximum power point current 2.94 A which is computed from the proposed GSS MPPT algorithm; maximum power

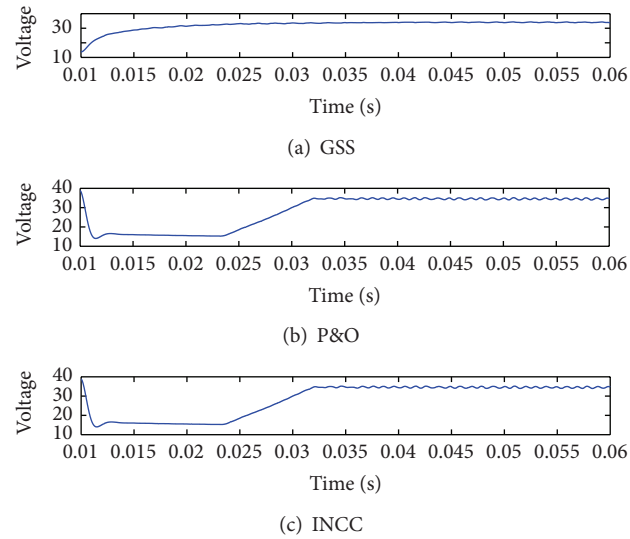

FIGURE 12: V_{ref} tracking using (a) GSS technique, (b) Perturb and Observe, and (c) Incremental Conductance with the given shading pattern.

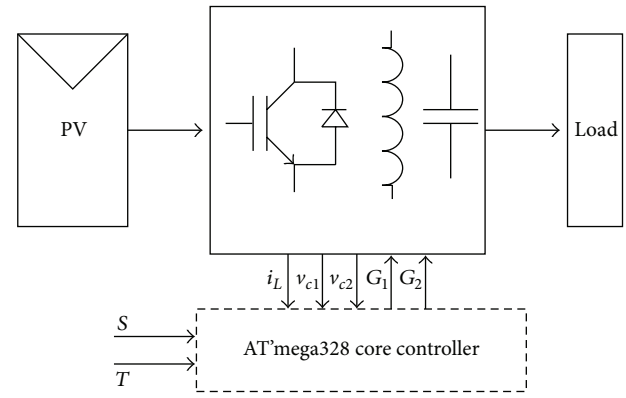

FIGURE 13: Block diagram of hardware prototype built.

100 W is reached within 0.5 s. The voltages across the capacitors are indicating different voltages and they are balanced as the controller is activated. The voltage balance across the two DC capacitors at 24 V is shown in Figure 16.

The level of the irradiation is also set to test the effectiveness of the GSS-MPPT controller. Figure 17 shows the controller tracking the maximum power with change in the current. The level of irradiation is changed from 800 W/m^2 to 1000 W/m^2 and the response of the GSS-MPPT algorithm is observed.

The voltage balancing loop is also tested under load change and response shown in Figure 18. The capacitor voltages are unbalanced before applying control loop. After enabling voltage balance control loop, both capacitor voltages v_{c1} and v_{c2} are converged to 24 V.

6.2. Performance Evaluation. The MPPT effectiveness is measured by measuring the efficiency. This is defined by the ratio of maximum power to the power tracking by MPPT. The proposed GSS based MPPT is evaluated for the efficiency. In

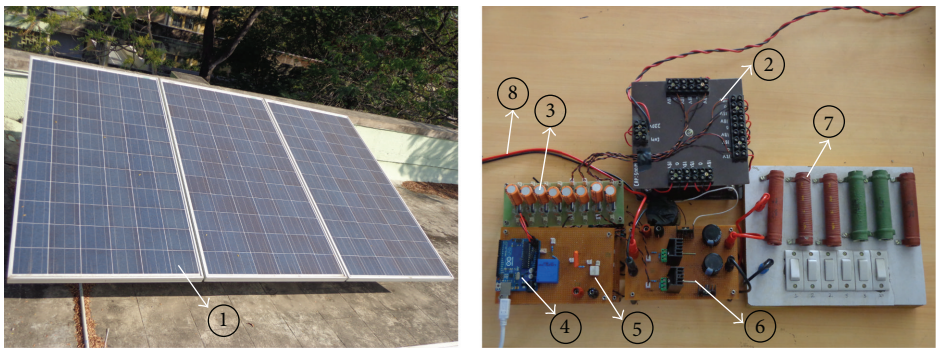

Figure 14: Prototype of the proposed PV energy conversion system. (1) Solar panels. (2) AC power supply for gate drivers. (3) TLP-250 based gate driver board. (4) At'mega328 controller. (5) Sensing circuitry board. (6) DC-DC converter power circuit. (7) Load. (8) Supply terminal from PV panel.

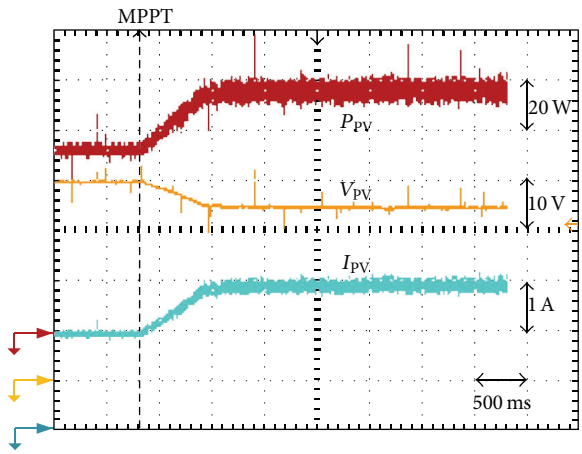

Figure 15: Performance of the DC/DC converter at start-up of MPPT.

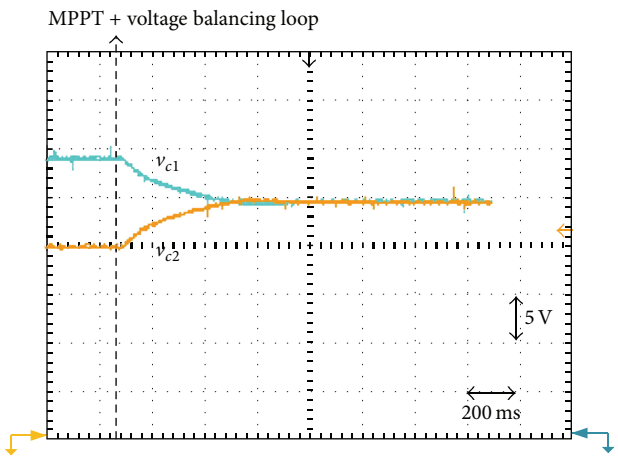

Figure 16: Voltages across capacitors with voltage balancing loop control.

simulation for $S = 1000\,\text{W/m}^2$, $T = 298\,\text{K}$, the maximum power is 100 W and tracking power using GSS MPPT is 99.8 W. The efficiency of the DC-DC converter is calculated for design values given in Table 2. The inductor ($L = 1.4\,\text{mH}$) used is found to have a resistance of 0.8 Ω and the efficiency obtained is 91%. The actual measured hardware efficiency for the 30 kHz operation is 89.7%. The variation of the inductor resistance by way of wire gauge selection influences the efficiency and it is indicated in Figure 19. Use of switching device and its switching frequency in a converter has a trade-off with the losses in the inductor. The operational efficiency of these converters can be achieved up to 98%.

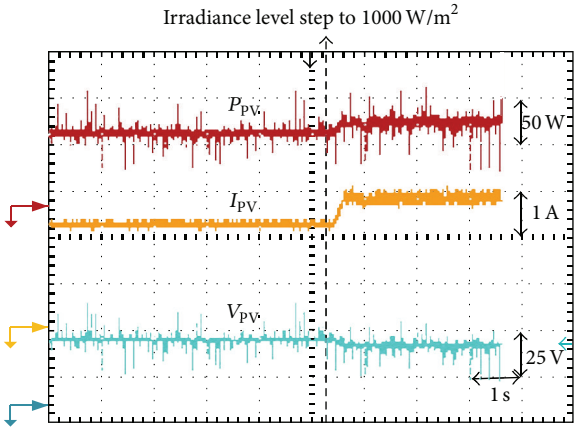

Figure 17: Dynamic response during change in irradiation from 800 to 1000 W/m^2.

7. Conclusion

The three-level boost converter is used to interface the PV system for maximization of the power extraction. The new maximum power point tracking algorithm based on the golden section search method is implemented. This algorithm shows the better dynamic response with the faster convergence without any oscillations while tracking. The voltage balancing of the DC bus is executed through the PI controller and performance is observed to be satisfactory. These controllers are implemented on the low cost AT'mega328 controller. The 100 W prototype is built to demonstrate the

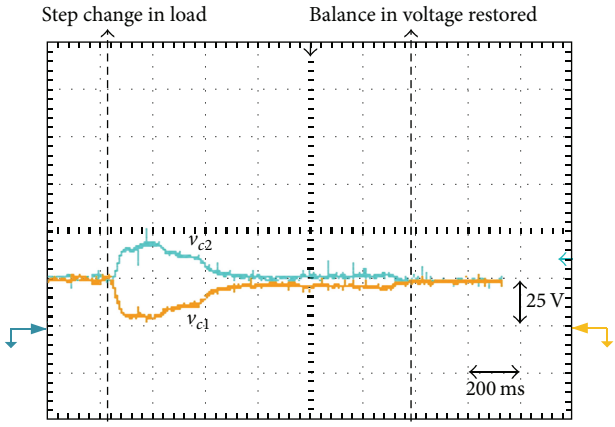

Figure 18: Capacitor voltage balance during load disturbance.

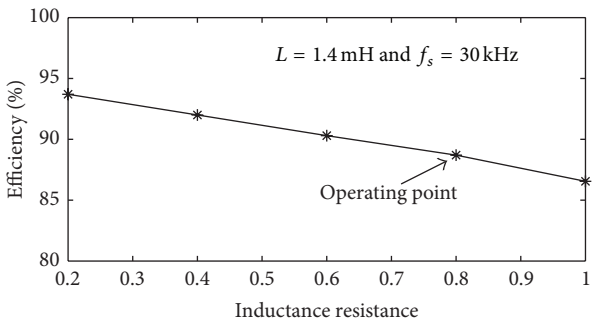

Figure 19: Variation in efficiency versus inductor parasitic resistance.

performance of this converter. The performance of the MPPT with GSS based algorithm indicates the good agreement with the simulated results. The steady state performance of the converter shows the balance voltage operation across the DC bus. It is indicated that the performance of the presented converter with varying irradiation as well as the load change is also in line with the simulation results. This indicates the converter performance with its efficiency up to 94% is achieved in these converters with high voltage gains in the PV energy conversion systems.

Conflict of Interests

The authors declare that there is no conflict of interests regarding the publication of this paper.

References

[1] M. Elshaer, A. Mohamed, and O. Mohammed, "Smart optimal control of DC-DC boost converter in PV systems," in *Proceedings of the IEEE/PES Transmission and Distribution Conference and Exposition: Latin America (T and D-LA '10)*, pp. 403–410, São Paulo, Brazil, November 2010.

[2] W. Li and X. He, "Review of non-isolated high-step-up DC/DC convertersin photovoltaic grid-connected applications," *IEEE Transactions on Industrial Electronics*, vol. 58, no. 4, pp. 1239–1250, 2011.

[3] B. Huang, A. Shahin, J. P. Martin, S. Pierfederici, and B. Davat, "High voltage ratio non-isolated DC-DC converter for fuel cell power source applications," in *Proceedings of the 39th IEEE Annual Power Electronics Specialists Conference (PESC '08)*, pp. 1277–1283, June 2008.

[4] A. M. Tuckey and J. N. Krase, "A low-cost inverter for domestic fuel cell applications," in *Proceedings of the IEEE 33rd Annual Power Electronics Specialists Conference (PESC '02)*, pp. 339–346, June 2002.

[5] C. Smith, M. Gilliom, D. Urciuoli, A. Mclandrich, E. Pepa, and J. S. Lai, "Low-cost solid oxide fuel cell power conditioning with bidirectional charging," in *Proceedings of the Fuel Cell Seminar*, pp. 8–15, Miami Beach, Fla, USA, November 2003.

[6] M. Velaerts, "New development of 3-level PWM strategies," in *Proceedings of the European Conference on Power Electronics and Applications*, 1989.

[7] O. Apeldoorn and L. Schulting, "10 kVA four level inverter with symmetrical input voltage distribution," in *Proceedings of the 5th European Conference on Power Electronics and Applications*, vol. 3, pp. 196–201, September 1993.

[8] M. T. Zhang, Y. Jiang, F. C. Lee, and M. M. Jovanovic, "Single-phase three-level boost power factor correction converter," in *Proceedings of the IEEE 10th Annual Applied Power Electronics Conference*, vol. 1, pp. 434–439, March 1995.

[9] C. Hua, C. Leu, Y. Jiang, and F. C. Lee, "Novel zero-voltage-transition PWM converters," *IEEE Transactions on Power Electronics*, vol. 9, no. 2, pp. 213–219, 1994.

[10] V. Yaramasu and B. Wu, "Three-level boost converter based medium voltage megawatt PMSG wind energy conversion systems," in *Proceedings of the 3rd Annual IEEE Energy Conversion Congress and Exposition (ECCE '11)*, pp. 561–567, Phoenix, Ariz, USA, September 2011.

[11] J.-M. Kwon, B.-H. Kwon, and K.-H. Nam, "Three-phase photovoltaic system with three-level boosting MPPT control," *IEEE Transactions on Power Electronics*, vol. 23, no. 5, pp. 2319–2327, 2008.

[12] E. Ribeiro, A. J. M. Cardoso, and C. Boccaletti, "Fault-tolerant strategyfor a photovoltaic DC-DC converter," *IEEE Transactions on Power Electronics*, vol. 28, no. 6, pp. 3008–3018, 2013.

[13] H.-C. Chen and W.-J. Lin, "MPPT and voltage balancing control with sensing only inductor current for photovoltaic-fed, three-level, boost-type converters," *IEEE Transactions on Power Electronics*, vol. 29, no. 1, pp. 29–35, 2014.

[14] A. N. A. Ali, M. H. M. Saied, M. Z. Mostafa, and T. M. Abdel-Moneim, "A survey of maximum PPT techniques of PV systems," in *Proceedings of the IEEE Energytech*, pp. 1–17, May 2012.

[15] J. Agrawal and M. Aware, "Golden section search (GSS) algorithm for maximum power point tracking in photovoltaic system," in *Proceedings of the IEEE 5th India International Conference on Power Electronics (IICPE '12)*, 6, p. 1, Delhi, India, December 2012.

[16] R. Shao and L. Chang, "A new maximum power point tracking method for photovoltaic arrays using golden section search algorithm," in *Proceedings of the IEEE Canadian Conference on Electrical and Computer Engineering (CCECE '08)*, pp. 619–622, May 2008.